

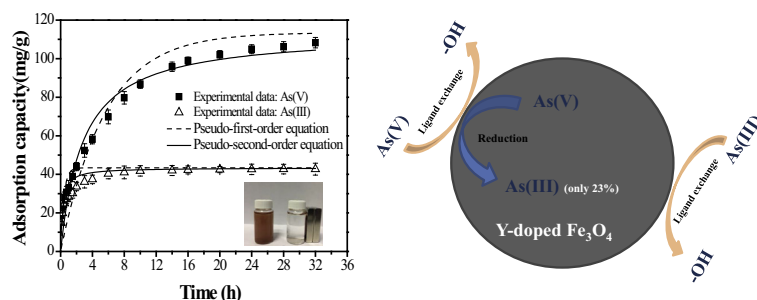


## Regular Article

## Yttrium-doped iron oxide magnetic adsorbent for enhancement in arsenic removal and ease in separation after applications

Yang Yu <sup>a,b</sup>, Ling Yu <sup>b,c</sup>, Kaimin Shih <sup>d</sup>, J. Paul Chen <sup>b,\*</sup><sup>a</sup> Guangdong Key Laboratory of Environmental Pollution and Health, and School of Environment, Jinan University, Guangzhou 510632, China<sup>b</sup> Department of Civil and Environmental Engineering, National University of Singapore, 10 Kent Ridge Crescent, Singapore 119260, Singapore<sup>c</sup> School of Environmental Science and Engineering, Sun Yat-Sen University, Guangzhou 510006, China<sup>d</sup> Department of Civil Engineering, The University of Hong Kong, Pokfulam Road, Hong Kong Special Administrative Region

## GRAPHICAL ABSTRACT



## ARTICLE INFO

## Article history:

Received 27 November 2017

Revised 14 February 2018

Accepted 15 February 2018

Available online 16 February 2018

## Keywords:

Adsorption

Arsenate

Arsenite

Yttrium

Magnetic adsorbent

Iron oxide

## ABSTRACT

Arsenic contamination is one of serious environmental problems in the world. In this study, an innovative yttrium-doped iron oxide magnetic adsorbent was synthesized through a simple precipitation method for better arsenic decontamination and ease in separation after the application. The adsorbent with a rough surface and porous structure was aggregated of nano-sized irregular particles after heat-drying procedure. The point of zero charge value of the adsorbent was about 7.0, giving good performance on the arsenate removal at weakly acidic and neutral conditions. The thermal gravimetric analysis, X-ray powder diffraction and X-ray photoelectron spectroscopy studies demonstrated that hydroxyl groups from goethite and amorphous species of the adsorbent were mainly responsible for the arsenic adsorption. The adsorption equilibrium of arsenate and arsenite was respectively established in 24 and 4 h. The maximum adsorption capacities of As(V) and As(III) at pH 7.0 were 170.48 and 84.22 mg-As/g, respectively. The better fit by the Freundlich isotherm indicated the mechanism of multi-layer adsorption for the removal. Our study demonstrated that the material would be suitable for treating arsenic-containing water with higher efficiency and ease in use.

© 2018 Elsevier Inc. All rights reserved.

## 1. Introduction

The risk of arsenic contamination in water can easily be found in many places in the world such as northern China, western

USA, India, and Vietnam. The arsenic exists in waters mainly in forms of As(V) and/or As(III). They are of great environmental importance because of the wide distribution in groundwater and some in surface water in the areas, and most importantly the higher toxicity than many other contaminants. Mainly present in groundwater, As(III) is at least 10 times more soluble and mobile than As(V). On the other hand, As(V) is the dominant form of

\* Corresponding author.

E-mail addresses: [paulchen@nus.edu.sg](mailto:paulchen@nus.edu.sg), [jpaulchen@gatech.edu](mailto:jpaulchen@gatech.edu) (J.P. Chen).

arsenic in surface water, and less toxic than As(III) [1]. As a series of severe health problems are due to arsenic exposure through drinking and food chains, arsenic is categorized as a primary contaminant strictly controlled by the World Health Organization (WHO) and environmental protection agencies such as USEPA.

Adsorption is effective for arsenic decontamination due to its higher efficiency, less expensive and easier operation than other technologies [2]. More than 50 types of adsorbents are available for arsenic removal. Difficulty in post-treatment is always of importance in industrial operations.

Magnetic adsorbents have attracted increasing attentions because they can more easily and rapidly be separated under an external magnetic field. Such magnetic materials as  $\text{Fe}_2\text{O}_3$  nanorods,  $\text{Fe}_3\text{O}_4$  nanoparticles, Fe-Pt alloy nanoparticles and  $\text{Fe}_3\text{O}_4$ -polymer composite were reported in the literatures [3–8]. In order to improve their adsorption ability towards arsenic, the magnetic materials are generally combined with other adsorptive materials such as activated carbon fiber [9], chitosan [10], reduced graphene/graphite oxide [11], clay [12] and other metal composites [13]. However, these magnetic adsorbents generally suffer from low adsorption capacity of arsenic. More importantly, they only work well in a narrow working pH range of 2–4, while industrial wastewater has a wider pH range of 1–13.

Recently, we reported the excellent performance of yttrium based adsorbents on removing arsenic. At pH 7.0, the adsorption capacities of hydrated yttrium oxide and yttrium-manganese binary metal oxide can respectively reach as high as 385.8 and 279.9 mg-As/g, much better than many adsorbents and ion exchange resins [14,15]. The high content of functional groups (e.g., hydroxyl group) bonded to yttrium atoms is responsible for their extremely high adsorption ability towards arsenic. Additionally, yttrium iron garnet (YIG) as a typical ferromagnetic material is widely studied because of its high resistivity, chemical stability and unique magneto-optical properties [16]. The substitution of yttrium was found to be beneficial for the improvement in the magnetic properties of NdFeB-type magnetic nanocomposites [17]. A new yttrium-doped iron oxide adsorbent can therefore be designed to achieve superior adsorption affinity towards arsenic and good magnetic properties.

In this study, a new yttrium-doped iron oxide magnetic adsorbent was synthesized by a simple precipitation method for arsenic decontamination. The adsorption performance was evaluated by a series of lab-scale experiments. The adsorbent structure and adsorption mechanism were investigated by field emission scanning electron microscope (FESEM), thermogravimetric analysis (TGA), X-ray powder diffraction (XRD) as well as X-ray photoelectron spectroscopy (XPS). The possible redox reaction between the magnetic components in the adsorbent and arsenite was discussed. It is anticipated that the findings from this study can provide new information on the material development for adsorption of arsenic. Interesting engineers may use the technology for industrial-scale water treatment of arsenic.

## 2. Material and methods

### 2.1. Materials

Iron(III) nitrate nonahydrate ( $\text{Fe}(\text{NO}_3)_3 \cdot 9\text{H}_2\text{O}$ , >98.0%), iron(II) sulfate heptahydrate ( $\text{FeSO}_4 \cdot 7\text{H}_2\text{O}$ , >99.0%), yttrium(III) nitrate hexahydrate ( $\text{Y}(\text{NO}_3)_3 \cdot 6\text{H}_2\text{O}$ , >99.8%), sodium hydroxide (NaOH, >98.0%), nitric acid ( $\text{HNO}_3$ , 70%), sodium phosphate monobasic ( $\text{NaH}_2\text{PO}_4$ , >99.0%), sodium sulfate ( $\text{Na}_2\text{SO}_4$ , >99.0%), sodium bicarbonate ( $\text{NaHCO}_3$ , >99.7%), sodium fluoride (NaF, >99.9%), arsenic(III) oxide ( $\text{As}_2\text{O}_3$ , >99.5%), sodium hydrogen arsenate heptahydrate ( $\text{Na}_2\text{HAsO}_4 \cdot 7\text{H}_2\text{O}$ , >99.5%) and humic acid sodium salt (HA, H16752) purchased from Sigma-Aldrich were used without further

purification. The stock solutions of As(V) and As(III) were respectively prepared by dissolving  $\text{Na}_2\text{HAsO}_4 \cdot 7\text{H}_2\text{O}$  and  $\text{As}_2\text{O}_3$  in deionized (DI) water.

### 2.2. Preparation of adsorbent

A mixture solution of  $\text{Y}(\text{NO}_3)_3 \cdot 6\text{H}_2\text{O}$ ,  $\text{Fe}(\text{NO}_3)_3 \cdot 9\text{H}_2\text{O}$  and  $\text{FeSO}_4 \cdot 7\text{H}_2\text{O}$  with molar ratio of 1:2:1 was used under continuous stirring at 80 °C in the adsorbent preparation. After that, NaOH solution was slowly dropwise added. The crystal particles were collected and washed by the DI water for several times. After heat-drying overnight, the adsorbent was grinded and finally stored for the study. In addition, an iron oxide was prepared through the same method as the adsorbent, so that it can be used for comparison with the virgin and As-loaded adsorbents in the XRD study.

### 2.3. Characterization of adsorbent

The point of zero charge (PZC) value was measured according to the reported method described as follows [18]. The adsorbent was dispersed in 0.01 M  $\text{NaNO}_3$  for 24 h, and then the pH of suspensions was respectively adjusted to a pH value of 3–10 by adding NaOH or  $\text{HNO}_3$ . After continuously stirring for 1 h, the pH value was measured and used as initial pH value. After that, a certain amount of  $\text{NaNO}_3$  was added to reach a concentration of 0.45 M. The suspensions were stirred for additional 3 h before measuring the final pH. The PZC was identified as the pH value, at which  $\Delta\text{pH}$  (final pH - initial pH) was zero in plot of  $\Delta\text{pH}$  and final pH.

FESEM was applied to investigate the morphology and structure of adsorbent (JSM6700F, JEQ, Japan). A thin layer of Pt was coated on the sample surface to improve electric conductivity. TGA (TA Instruments, 2960 SDT V3.0F) was carried out in the temperature range of 25–800 °C with a heating rate of 10 °C/min under a  $\text{N}_2$  atmosphere.

XRD measurements were performed for understanding the adsorbent structure. The  $2\theta$  scan range was from 10 to 80° with a step size of 0.02° and counting time of 0.2 s. The composition of samples was analyzed by using the Rietveld quantitative analysis with a spiking internal standard. The samples were first mixed with 15 wt% of  $\text{CaF}_2$  (449717-25G, Merck, Germany). The Rietveld quantitative XRD analysis was finally conducted by using a software of TOPAS4.2 (Bruker AXS GmbH, Germany).

Surface element valence states and adsorption mechanism of the adsorbent were determined by XPS (Kratos XPS system-Axis His-165 Ultra, Shimadzu, Japan). The XPS spectra were fitted with linear backgrounds and mixed functions composed of Gaussian (20%) and Lorentzian (80%) by using XPSPEAK 41 Software. In order to compensate any charging effect, all spectra were corrected according to the binding energy of the C 1 s of graphite carbon (assigned to 284.8 eV).

### 2.4. Adsorption experiments

The pH effect study was conducted in the pH range of 3–10. The initial concentration of arsenic ( $[\text{As}]_0$ ) was set at 20 mg-As/L. The adsorbent dosage ( $m$ ) was 0.1 g/L. After agitation for 24 h at room temperature, arsenic concentration was measured by using an inductively coupled plasma optical emission spectrometer (ICP-OES, PerkinElmer Optima 3000).

In the adsorption kinetics study, the solution pH was maintained at 7.0 during the adsorption process. Samples were collected at different time intervals for determination of arsenic concentration.

In the adsorption isotherm experiments, the adsorbent was respectively added into arsenic solutions with different concentra-

tions ranging from 1 to 100 mg-As/L. After 24-h adsorption process, arsenic concentration was measured.

In order to investigate the influence of competitive substances,  $\text{NaH}_2\text{PO}_4$ ,  $\text{Na}_2\text{SO}_4$ , NaF,  $\text{NaHCO}_3$  and HA were respectively added into 20-mg/L arsenic solutions. The adsorbent dosage was 0.1 g/L and solution pH was maintained at 7.0. After 24-h agitation, the arsenic concentration was measured.

The reusability of the adsorbent was evaluated by regeneration experiments. The used adsorbent was separated by an external magnetic field and then treated by a 0.5-M NaOH solution under shaking for 6 h. The regenerated adsorbent was washed, dried in the oven and used for next cycle of adsorption experiment. Three cycles of regeneration experiments were carried out in this study.

### 3. Results and discussion

#### 3.1. Characterization of adsorbent

As shown in Fig. 1a, the adsorbent with rough surface morphology is aggregated of nano-sized particles after the heat-drying procedure. This structure should be beneficial for the diffusion of arsenic inside the adsorbent.

The separation ability of the adsorbent under an external magnetic field is shown in Fig. 1b. The dispersed adsorbent in solution can be rapidly separated from water under the help of an external magnetic field.

Thermogravimetric analysis was used to identify the change in functional groups on adsorbents before and after adsorption. Fig. 1c shows that only a slight difference in mass (%) of virgin and As-loaded adsorbents is observed.

The As-loaded adsorbent shows a slightly more mass loss at the temperature below 300 °C than the virgin adsorbent. At the temperature above 300 °C, the trend becomes reverse. As reported,

the loss of physically adsorbed water and lattice water occurs in the temperature range of 25–100 °C and 100–300 °C, respectively, while the hydroxyl group disappears at the temperature above 300 °C [19]. These observations indicate that some of hydroxyl groups on the adsorbent surface might be replaced by arsenic species after the adsorption.

As shown in Fig. 1d, the value of PZC is approximately 7.0. The adsorbent surface is protonated at  $\text{pH} < 7.0$ . This indicates further that the adsorbent would work well at  $\text{pH} < 7$ . The interactions (e.g., adsorption reaction and electrostatic attraction) between the anionic arsenic and the protonated adsorbent are therefore enhanced, which finally facilitate the arsenic diffusion towards the adsorbent. In contrast, the deprotonated adsorbent surface would hinder the uptake of As(V) and As(III) to some extent when pH is above 7.0.

An iron oxide was prepared through the same method as the adsorbent. As shown in Fig. 2, two crystalline phases, magnetite ( $\text{Fe}_3\text{O}_4$ ) and goethite ( $\text{FeOOH}$ ), are mainly involved in the iron oxide. According to the XRD profile analysis with the fundamental parameter approach, the crystal size of both magnetite and goethite is around 10 nm.

The Rietveld quantitative analysis with the spiking internal standard was also applied to quantify the contents of magnetite, goethite and the amorphous. The result shows that the contents of amorphous iron oxide, magnetite and goethite are 35.1, 35.6 and 29.3 wt.%, respectively.

In the XRD pattern of the virgin adsorbent, only a broaden peak is observed at about 35°. This indicates that the adsorbent is poorly crystallized. The crystals could be of nano-sized (<5 nm). The different structures between the iron oxide and the adsorbent may be caused by the addition of yttrium salts. The existence of Y(III) may hinder the crystallization process during it was being prepared. There is no difference in XRD patterns of adsorbents before

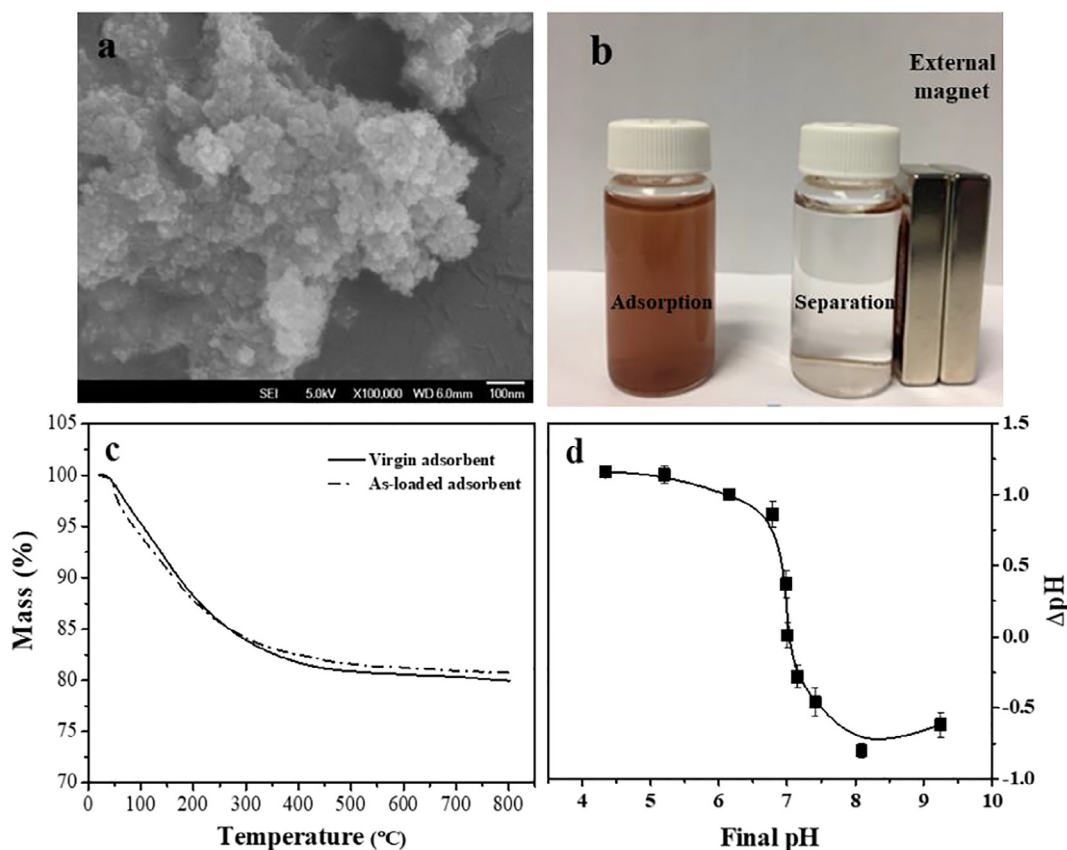


Fig. 1. Characterization of adsorbents: (a) FESEM image; (b) separation of adsorbent after use; (c) TGA images; (d) PZC.

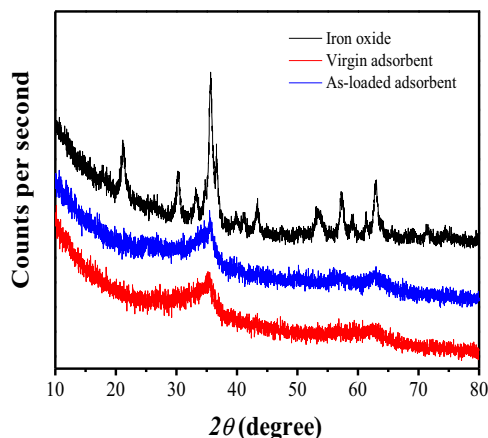


Fig. 2. XRD patterns of prepared iron oxide, and virgin and As-loaded adsorbents.

and after the adsorption; this demonstrates that the arsenic is adsorbed on the adsorbent surface without affecting the adsorbent's crystal structure. According to the XRD results as mentioned above, the hydroxyl groups from the goethite, and the surface of amorphous and partially crystallized magnetite may participate in the adsorption of arsenic.

### 3.2. Adsorption kinetics

As shown in Fig. 3a, the adsorption of As(V) and As(III) can proceed rapidly at the beginning and the equilibrium is reached within 24 and 4 h, respectively. About 60% of the ultimate adsorption of As(III) (25 mg-As/g) is achieved in the initial 30 min, indicating that the yttrium-doped iron oxide adsorbent could be used as a promising adsorptive material for treating arsenite contaminated groundwater. It takes about 5 h to reach the same removal of 60% if the adsorbate is arsenate.

The pseudo-first- and pseudo-second-order equations were applied to simulate the adsorption process. As shown in Fig. 3a and Table 1, better fit of the pseudo-second-order model indicates that the arsenic adsorption is governed by chemisorption process [20]. The  $K_1$  value of As(III) adsorption is apparently higher than that of As(V), suggesting that faster adsorption kinetics of As(III) occurs on adsorbent surface. Different from other studies [13,21], a relatively slower adsorption of As(V) than As(III) is observed. This may be due to the occurrence of the As(V) reduction on the adsorbent surface (to be discussed later).

The intraparticle diffusion model was employed to identify rate-controlling step of adsorption process. If the plot of adsorption capacity against  $t^{1/2}$  gives a straight line, the intraparticle diffusion would be the controlling step [9,22–24]. The plots of adsorption capacities of As(V) and As(III) versus  $t^{1/2}$  are illustrated in Fig. 3b. The intraparticle diffusion rate constant ( $k_{id}$ ) can be obtained from the slope of the linear portion. The intercept of the plot ( $\alpha$ ) gives an insight into the effect of the boundary layer on the rate-limiting step.

As illustrated in Table 1, the adsorption process is likely to be controlled by the intraparticle diffusion. Since the adsorbent is neutrally charged at pH 7.0, the electrostatic interaction between adsorbent and arsenic species should be negligible. A similar boundary layer effect is observed during the adsorption of As(V) and As(III).

### 3.3. pH effect

Adsorption efficiency of the adsorbent towards As(V) and As(III) is highly affected by solution pH as shown in Fig. 4. The As(V)

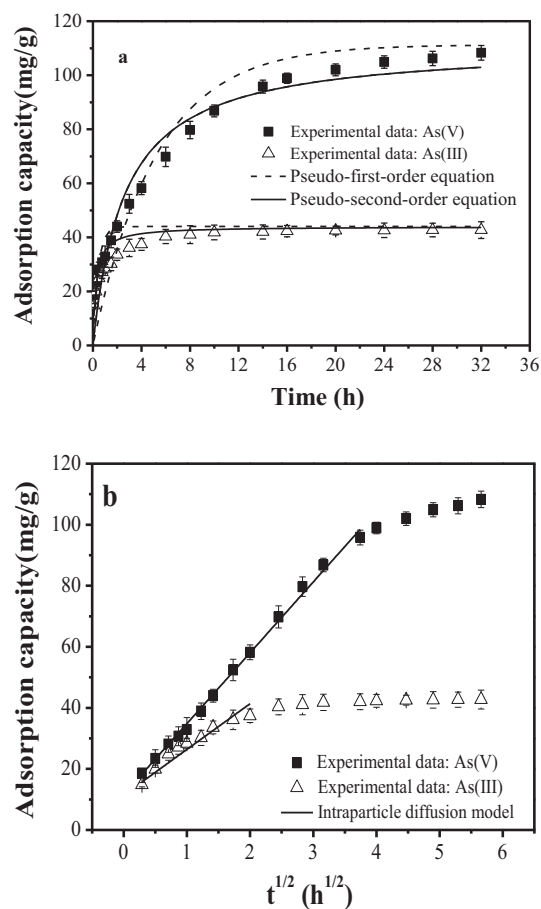


Fig. 3. Adsorption kinetics of arsenic removal by the adsorbent: (a) experimental data and modeling results from pseudo-first-order and pseudo-second-order equations; (b) intraparticle diffusion model. Experiment conditions:  $[As]_0 = 20$  mg-As/L;  $m = 0.1$  g/L; pH = 7.0,  $T = 25 \pm 1$  °C.

uptake reaches the optimal value of 172.2 mg-As/g at pH 4.0, and then significantly decreases. In contrast, the uptake of As(III) increases as solution pH is increased from 3 to 8.0. After that, a slight reduction is observed.

The pH effect on the removal is caused by the speciation of As(V) and As(III) under different pH and the surface properties of the adsorbent. As shown in Fig. S1, the dominant forms of As(V) are negatively charged  $H_2AsO_4^-$  and  $HAAsO_4^{2-}$  in the tested pH range, while As(III) respectively exists in form of neutrally charged  $H_3AsO_3$  at pH < 8.0 and negatively charged  $H_2AsO_3^-$  at pH > 8.0. Since the adsorbent becomes protonated at pH < 7.0 according to its PZC value, stronger electrostatic attraction and adsorption reactions become favourable for the removal of As(V). In contrast, the As(V) adsorption is retarded at pH > 7. More importantly, the ligand exchange between arsenic species and  $-OH_2^+$  group is reportedly more favorable than  $-OH$  or  $-O^-$  groups, since  $-OH_2^+$  group is more conducive to depart from the metal atoms [25]. Similarly, the decrease in uptake of As(III) at pH > 8.0 is likely due to electrostatic repulsion between As(III) and deprotonated adsorbent.

### 3.4. Adsorption isotherm

The adsorption isotherms at pH 7.0 are shown in Fig. 5. One can see that the adsorbent shows excellent adsorption for both As(V) and As(III).

As summarized in Table 2, the Freundlich isotherm works better to fit the experimental data than the Langmuir isotherm. Similar

**Table 1**  
Constants of adsorption kinetics models.

	Pseudo-first-order			Pseudo-second-order			Intraparticle diffusion		
	$q_e$ (mg/g)	$K_1$ ( $\text{h}^{-1}$ )	$r^2$	$q_e$ (mg/g)	$K_2$ ( $\text{g}\cdot\text{mg}^{-1}\cdot\text{h}^{-1}$ )	$r^2$	$k_{id}$ ( $(\text{mg}/\text{g})/\text{h}^{1/2}$ )	$\alpha$ (mg/g)	$r^2$
As(V)	111.3	0.192	0.89	111.3	0.003	0.94	23.21	11.62	0.99
As(III)	44.0	2.39	0.67	44.0	0.089	0.89	14.98	11.41	0.98

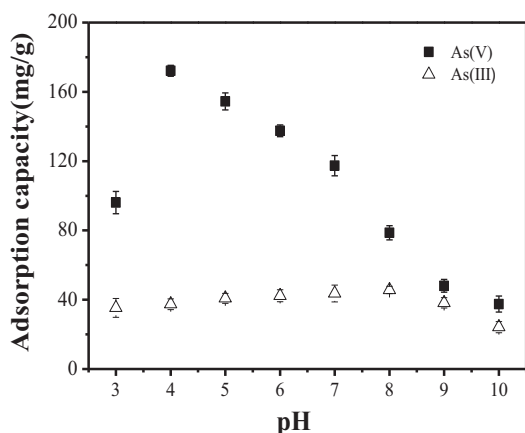


**Fig. 4.** Effect of solution pH on arsenic uptake. Experiment conditions:  $[\text{As}]_0 = 20$  mg-As/L;  $m = 0.1$  g/L;  $T = 25 \pm 1$  °C.

finding was reported for the arsenic adsorption on cetyltrimethylammonium bromide (CTAB) modified magnetic nanoparticles [26].

The Freundlich isotherm is more suitable than the Langmuir isotherm for multilayer adsorption onto the surface of heterogeneous sites with different bonding energies. The result shows that more than one type of adsorption sites on the adsorbent contribute to the arsenic removal.

On the basis of XRD results, the hydroxyl groups from goethite may participate in the arsenic adsorption. Additionally, the adsorption ability of the  $\text{Fe}_3\text{O}_4$  particle towards arsenic has been well recognized, with the varied adsorption capacity of 0.75–172.5 mg-As/g [27]. Therefore, the magnetic component in the adsorbent may provide a certain number of active sites for arsenic adsorption. In the adsorption, arsenic can be bonded on the adsorbent surface via the linkages of Y-O-As and Fe-O-As.

The Freundlich constants,  $K_f$  and  $1/n$ , are related to the adsorption capacity and adsorption intensity, respectively. The adsorption would be favorable when  $0.5 < 1/n \leq 1$ , and more favorable when  $0.1 < 1/n < 0.5$ . However, the adsorption would be considered to be unfavorable as  $1/n > 1$  [28]. The values of  $1/n$  for the As(V) and As(III) adsorption are respectively calculated to be 0.22 and 0.38 as listed in Table 2, demonstrating that As(V) and As(III) can be quite easily adsorbed on the adsorbent.

The maximum adsorption capacities of As(V) and As(III) calculated from the Langmuir isotherm are 170.48 and 84.22 mg-As/g, respectively. On the basis of the relative contents of different elements and the percentages of oxygen-containing groups in Table S1, the theoretical content of hydroxyl group in the adsorbent is calculated as 4.92 mmol/g. If arsenic species can be replaced (be exchanged) with the hydroxy group with a molar ratio of 1:1, the ideal maximum adsorption capacity should be 368.8 mg-As/g.

The maximum adsorption capacity is highly affected by such solution properties as pH, co-existing ions and ion strength, and surface properties of adsorbent [33–38]. A comparison between the yttrium-doped iron oxide adsorbent and other magnetic adsorbents previously reported is illustrated in Fig. 6. The adsorption capacities for As(III) and As(V) of our adsorbent are several times higher than others. The adsorption capacity of iron oxide towards arsenic is significantly enhanced by the yttrium doping. Additionally, the functional components in the heterogeneous structure of the material can synergistically promote the adsorption activity for arsenic.

The adsorption capacities of the adsorbent in three cycles of adsorption/desorption experiments are shown in Fig. S2. The value in Cycle 0 represents the adsorption capacity of the virgin adsorbent. After the first cycle of regeneration, about 85.8% and 76.7% of adsorption capacities can be recovered for As(V) and As(III), respectively. The adsorption capacity for As(V) and As(III) after three cycles of regeneration could respectively reach 64.0% and 52.7%.

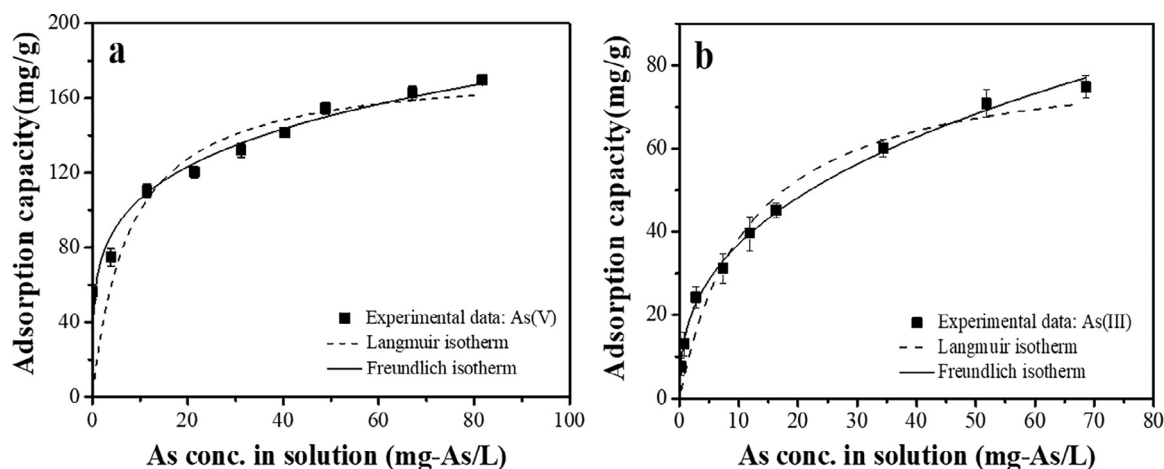


**Fig. 5.** Adsorption isotherm of arsenic on the adsorbent. Experiment conditions:  $\text{pH} = 7.0$ ;  $m = 0.1$  g/L;  $T = 25 \pm 1$  °C.

**Table 2**  
Isotherm parameters for the arsenic adsorption.

	Langmuir isotherm			Freundlich isotherm		
	$q_{max}$ (mg/g)	$b$ (L/mg)	$r^2$	$K_f$ (mg <sup>(1-1/n)</sup> L <sup>1/n</sup> /g)	1/n	$r^2$
As(V)	170.48	0.16	0.687	63.82	0.22	0.958
As(III)	84.22	0.09	0.949	15.34	0.38	0.996

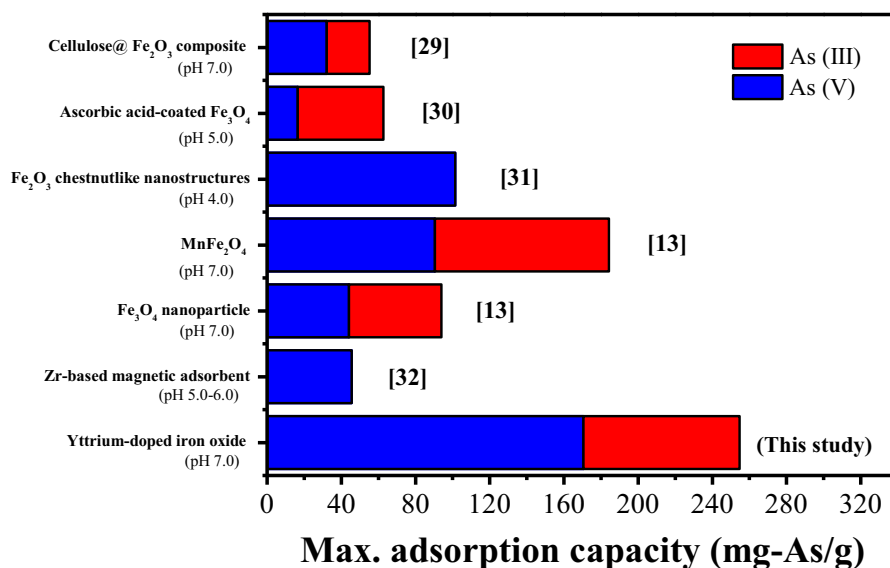


**Fig. 6.** Comparison of arsenic adsorption performance among different iron oxide based adsorbents. (See above-mentioned references for further information.)

Since the adsorption capacity is much higher than other magnetic adsorbents, the adsorbent dosage would be less than other adsorbents in the water treatment. This finding clearly demonstrates that the developed material has a more promising potential for arsenic decontamination.

### 3.5. Effect of competitive substances

Several anions such as bicarbonate, sulphate, fluoride and phosphate and natural organic matter (NOM) well exist in waters. It is of importance to find out whether their presence can affect the performance of adsorbent.

As shown in Fig. 7, the effect of competitive substances on the adsorption follows the order of:  $\text{HPO}_4^{2-}/\text{H}_2\text{PO}_4^- > \text{F}^- \gg \text{HA} > \text{SO}_4^{2-} > \text{HCO}_3^-$ . The presence of phosphate causes the most significant influence on the adsorption. When 1-mM phosphate exists in waters, the uptake of As(V) and As(III) decreases by 64.1% and 42.4% respectively. The strong competition of phosphate with arsenic species is attributed to the fact that they are similar to each in terms of chemical properties [39].

Note that the typical concentration of phosphate in natural waters is generally lower than 0.15 mM [40]. The adsorption capacities of As(V) and As(III) are respectively still above 74.5 and 31.4 mg-As/g at concentration of phosphate at 0.1 mM.

The presence of fluoride can also retard the arsenic removal as shown in the figure. Our previous study showed high affinity of yttrium-based adsorbents towards fluoride [14,15]. Fluoride with the highest electronegativity in the periodic table of elements can form a stronger covalent bond with metal atoms (e.g., Y or Fe in the adsorbent) than hydroxyl group (-OH). As such, there is co-adsorption of both arsenic and fluoride, leading to the reduction in the arsenic uptake. Compared to phosphate and fluoride, the existence of sulphate, bicarbonate and HA only slightly depresses the uptake of As(V) and As(III).

### 3.6. Mechanism study

XPS analysis was applied to determine the valence state of elements and the interaction between As(V) and functional groups on the adsorbent. As one can see from XPS wide-scan spectra of adsorbents before and after the As(V) adsorption (Fig. 8), four peaks of Y 4p, Y 4s, Y 3d and Y 3p and two peaks of Fe 2p and Fe LMM can be detected on both virgin and As(V)-loaded adsorbents. After the adsorption, the appearance of As 3d, As 3s and As LMM peaks confirms the loading of arsenic.

To better understand structural changes of the adsorbent after the adsorption, the high-resolution XPS spectra of As 3d, Y 3d, Fe 2p and O 1s were investigated with results given in Fig. 9 and Table S1. As shown in Fig. 9a, the high resolution XPS spectrum of As 3d is composed of two characteristic peaks with binding energies of 45.2 and 46.1 eV corresponding to As(III) and As(V), respectively [32,41]. On the basis of the relative contents listed in Table S1, approximately 23.4% of the As(V) on adsorbent surface has been reduced to As(III).

As shown in Fig. S3a, the characteristic peak of yttrium can be decomposed into two component peaks with the binding energies of ~158 and ~160 eV, which are assigned to Y 3d<sub>5/2</sub> and Y 3d<sub>3/2</sub>, respectively. After the adsorption, the positions of yttrium peaks shift to higher levels due to the bonding of more electronegative As(V) ions. Meanwhile, the valence state of yttrium element on the adsorbent is not changed, indicating the yttrium atoms would not participate in redox reaction. According to the peak intensity of Y and Fe elements as listed in Table S1, the real molar ratio of Y/Fe in the virgin adsorbent is about 0.29 and slightly decreases to 0.28 after the adsorption.

XPS spectra given in Fig. S3b demonstrate that iron element in the adsorbent has two oxidation states, Fe(II) and Fe(III) [42]. The peak at the lowest binding energy of 710.4 eV and its corresponding satellite peak at 7163.0 eV are assigned to Fe(II), while the

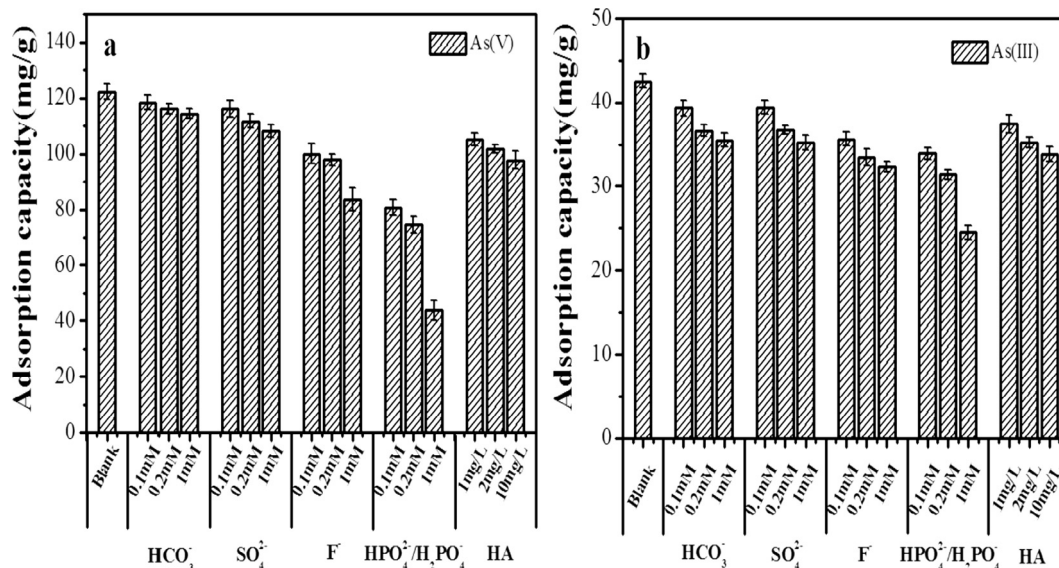


Fig. 7. Effects of competitive anions and HA on arsenic uptake. Experiment conditions:  $[As]_0 = 20$  mg-As/L;  $m = 0.1$  g/L;  $T = 25 \pm 1$  °C;  $pH = 7.0$ .

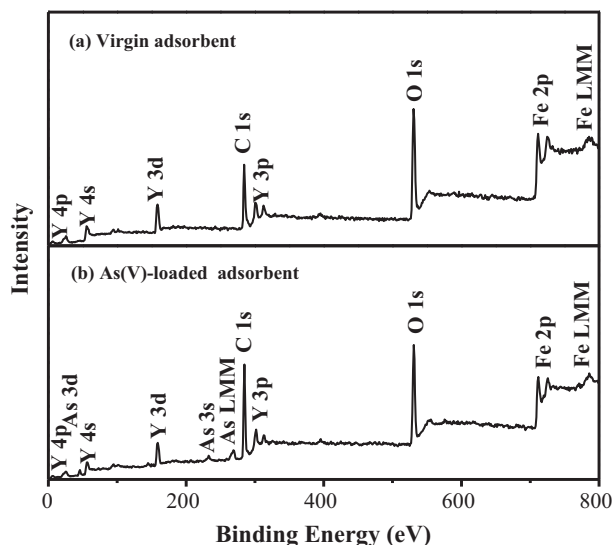


Fig. 8. XPS wide-scan spectra of the adsorbents before and after As(V) adsorption.

peaks of  $Fe(III)_{oct}$  and  $Fe(III)_{tet}$  can be observed at binding energies of 711.7 and 713.3 eV, respectively [43]. Based on the relative contents of Fe(II) and Fe(III) in Table S1, the molar ratio of Fe(II)/Fe(III) in virgin adsorbent is calculated to be 0.46, close to the expected value of 0.5 for  $Fe_3O_4$  particles. Similar to yttrium, binding energies of iron element also shift to higher levels after the adsorption. This is consistent with the results from isotherm study that arsenic can be bonded on both yttrium and iron atoms. Moreover, the Fe(II)/Fe(III) ratio decreases to 0.41 after the adsorption; this indicates that Fe(II) is partially oxidized to Fe(III).

As shown in Fig. 9b, the O 1s spectrum of the virgin adsorbent is composed of three component peaks, which are respectively assigned to the metal-oxide (M-O), the metal-hydroxyl group (M-OH) and the adsorbed water ( $H_2O$ ). After the As(V) adsorption, the relative content of M-OH significantly decreases from 56.6% to 43.9%, while the contents of M-O and  $H_2O$  increase from 33.0% and 10.4% to 34.1% and 22.0%, respectively (as listed in Table S1). These results provide a clear evidence for the role of hydroxyl groups in arsenic uptake. In our previous studies, abundant hydroxyl groups on the surface of yttrium-based adsorbents can be exchanged by

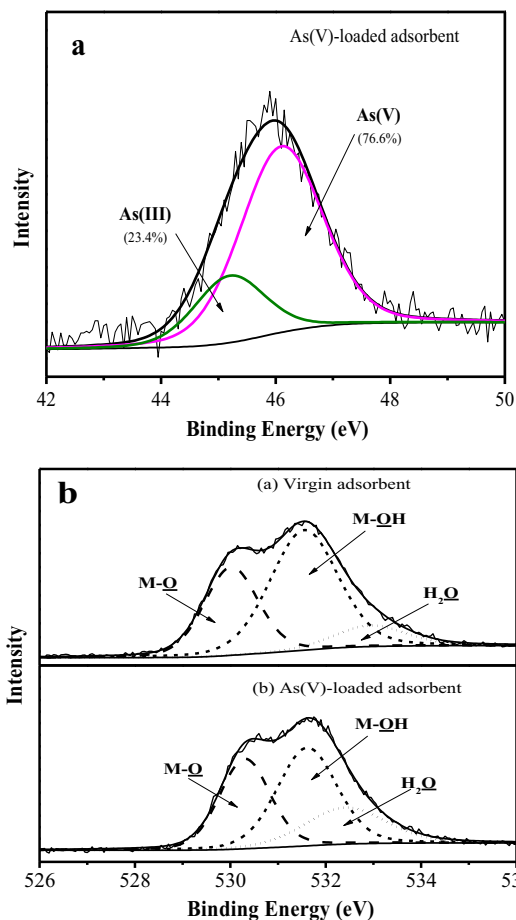
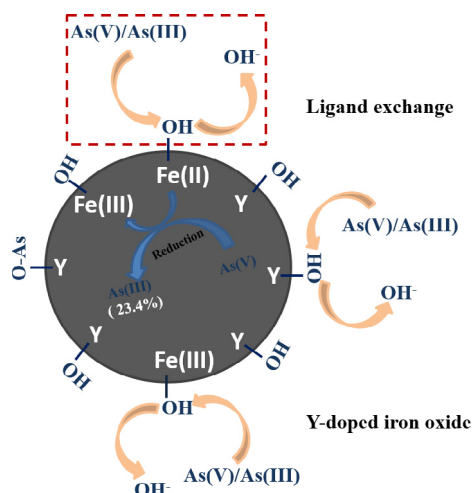


Fig. 9. High-resolution XPS spectra of the adsorbents before and after adsorption: (a) As 3d; and (b) O 1s.

arsenic species [14,15]. The formation of the hydroxyl groups is due to the poor crystallization of the nano-sized yttrium-based adsorbent, which is revealed by XRD results shown in Fig. 2.

As shown in Fig. 10, the mechanism of arsenic adsorption can be deduced to be a synergistic process involving the exchange



**Fig. 10.** Schematic diagram of adsorption and redox mechanism involved in adsorption process.

between hydroxyl groups and arsenic species and partial reduction of As(V) to As(III). The arsenic is effectively adsorbed via the linkages of Y-O-As and Fe-O-As.

#### 4. Conclusions

A new yttrium-doped iron oxide adsorbent was reported for great arsenic removal with ease in separation after use. The adsorbent with a rough surface was aggregated of irregular nanoparticles. The uptake of the arsenic was highly pH-dependent. As(III) was more rapidly adsorbed than As(V). The adsorbent had the maximum adsorption capacity of 170.48 mg-As/g for As(V) and 84.22 mg-As/g for As(III) at pH 7.0, several folds higher than those reported magnetic adsorbents. The better fit to the Freundlich isotherm demonstrated the presence of more than one types of adsorption sites for arsenic adsorption. The presence of phosphate and fluoride had great impact on the adsorption as they could also be adsorbed onto the adsorbent.

The XPS analysis showed that both the adsorption and redox reaction occurred during the adsorption process. The hydroxyl groups played the key role in the arsenic removal via the ligand exchange mechanism. Compared to other magnetic adsorbents, the yttrium-doped iron oxide adsorbent can be produced in a simple and cost-effective method. Its applications in industrial-scale treatment of arsenic-rich wastewater should be studied in the near future. This type of adsorbents together with others may provide a good solution for treatment of small-volume metal containing wastewater [44].

#### Acknowledgments

Y.Y appreciates National University of Singapore for providing President's Graduate Scholarship during his Ph.D study. This research/project is supported by the National Research Foundation, Prime Minister's Office, Singapore under its Campus for Research Excellence and Technological Enterprise (CREATE) programme.

#### Appendix A. Supplementary material

Supplementary data associated with this article can be found, in the online version, at <https://doi.org/10.1016/j.jcis.2018.02.046>.

#### References

- [1] M.A. Rahman, M.A. Rahman, A. Samad, A.S. Alam, Removal of arsenic with oyster shell: experimental measurements, *Pak. J. Anal. Environ. Chem.* 9 (2) (2008) 9.
- [2] D. Mohan, C.U. Pittman, Arsenic removal from water/wastewater using adsorbents—a critical review, *J. Hazard. Mater.* 142 (1) (2007) 1–53.
- [3] M. Perovic, V. Kusigerski, A. Mrakovic, V. Spasojevic, J. Blanus, V. Nikolic, O. Schneeweiss, B. David, N. Pizurova, The glassy behaviour of poorly crystalline Fe<sub>2</sub>O<sub>3</sub> nanorods obtained by thermal decomposition of ferrous oxalate, *Nanotechnology* 26 (11) (2015) 115705.
- [4] K.R. Reddy, K.P. Lee, A.I. Gopalan, Novel electrically conductive and ferromagnetic composites of poly(aniline-co-aminonaphthalenesulfonic acid) with iron oxide nanoparticles: synthesis and characterization, *J. Appl. Polym. Sci.* 106 (2) (2007) 1181–1191.
- [5] K.R. Reddy, K.P. Lee, A.I. Gopalan, S.K. Min, A.M. Showkat, Y.C. Nho, Synthesis of metal (Fe or Pd)/alloy (Fe-Pd)-nanoparticles-embedded multiwalled carbon nanotube/sulfonated polyaniline composites by  $\gamma$  irradiation, *J. Polym. Sci., Part A: Polym. Chem.* 44 (10) (2006) 3355–3364.
- [6] K.R. Reddy, K.P. Lee, A.I. Gopalan, Self-assembly directed synthesis of poly(ortho-toluidine)-metal(gold and palladium) composite nanospheres, *J. Nanosci. Nanotechnol.* 7 (9) (2007) 3117–3125.
- [7] K.R. Reddy, B.C. Sin, H.Y. Chi, W. Park, K.S. Ryu, J.S. Lee, D. Sohn, Y. Lee, A new one-step synthesis method for coating multi-walled carbon nanotubes with cuprous oxide nanoparticles, *Scr. Mater.* 58 (11) (2008) 1010–1013.
- [8] K.R. Reddy, W. Park, B.C. Sin, J. Noh, Y. Lee, Synthesis of electrically conductive and superparamagnetic monodispersed iron oxide-conjugated polymer composite nanoparticles by in situ chemical oxidative polymerization, *J. Colloid Interface Sci.* 335 (1) (2009) 34–39.
- [9] S. Zhang, X.Y. Li, J.P. Chen, Preparation and evaluation of a magnetite-doped activated carbon fiber for enhanced arsenic removal, *Carbon* 48 (1) (2010) 60–67.
- [10] L.C.B. Stopa, M. Yamaura, Uranium removal by chitosan impregnated with magnetite nanoparticles: adsorption and desorption, *Int. J. Nucl. Energy Sci. Technol.* 5 (4) (2010) 283–289.
- [11] V. Chandra, J. Park, Y. Chun, J.W. Lee, I.C. Hwang, K.S. Kim, Water-dispersible magnetite-reduced graphene oxide composites for arsenic removal, *ACS Nano* 4 (7) (2010) 3979–3986.
- [12] L.C.A. Oliveira, R.V.R.A. Rios, J.D. Fabris, K. Sapag, V.K. Garg, R.M. Lago, Clay-iron oxide magnetic composites for the adsorption of contaminants in water, *Appl. Clay Sci.* 22 (4) (2003) 169–177.
- [13] S. Zhang, H. Niu, Y. Cai, X. Zhao, Y. Shi, Arsenite and arsenate adsorption on coprecipitated bimetal oxide magnetic nanomaterials: MnFe<sub>2</sub>O<sub>4</sub> and CoFe<sub>2</sub>O<sub>4</sub>, *Chem. Eng. J.* 158 (3) (2010) 599–607.
- [14] Y. Yu, L. Yu, J.P. Chen, Introduction of an yttrium-manganese binary composite that has extremely high adsorption capacity for arsenate uptake in different water conditions, *Ind. Eng. Chem. Res.* 54 (11) (2015) 3000–3008.
- [15] Y. Yu, L. Yu, M. Sun, J.P. Chen, Facile synthesis of highly active hydrated yttrium oxide towards arsenate adsorption, *J. Colloid Interface Sci.* 474 (2016) 216–222.
- [16] M. Gharibshahi, A. Hasanpour, M. Niyafefar, Study of magneto-optical characteristics of cerium incorporated yttrium iron garnet films, *Mater. Res. Bull.* 99 (2018) 219–224.
- [17] Z. Chen, J. Luo, Y. Sui, Z. Guo, Effect of yttrium substitution on magnetic properties and microstructure of Nd-Y-Fe-B nanocomposite magnets, *J. Rare Earths* 28 (2) (2010) 277–281.
- [18] C.J. Kuo, G.L. Amy, C.W. Bryant, Factors affecting coagulation with aluminum sulfate-I. Particle formation and growth, *Water Res.* 22 (7) (1988) 853–862.
- [19] Y. Ma, Y.M. Zheng, J.P. Chen, A zirconium based nanoparticle for significantly enhanced adsorption of arsenate: synthesis, characterization and performance, *J. Colloid Interface Sci.* 354 (2) (2011) 785–792.
- [20] V. Vimonse, S. Lei, B. Jin, C.W. Chow, C. Saint, Kinetic study and equilibrium isotherm analysis of Congo Red adsorption by clay materials, *Chem. Eng. J.* 148 (2) (2009) 354–364.
- [21] G. Zhang, Z. Ren, X. Zhang, J. Chen, Nanostructured iron(III)-copper(II) binary oxide: a novel adsorbent for enhanced arsenic removal from aqueous solutions, *Water Res.* 47 (12) (2013) 4022–4031.
- [22] V. Vadivelan, K.V. Kumar, Equilibrium, kinetics, mechanism, and process design for the sorption of methylene blue onto rice husk, *J. Colloid Interface Sci.* 286 (1) (2005) 90–100.
- [23] G. Walker, L. Hansen, J.A. Hanna, S. Allen, Kinetics of a reactive dye adsorption onto dolomitic sorbents, *Water Res.* 37 (9) (2003) 2081–2089.
- [24] F.C. Wu, R.L. Tseng, R.S. Juang, Initial behavior of intraparticle diffusion model used in the description of adsorption kinetics, *Chem. Eng. J.* 153 (1) (2009) 1–8.
- [25] Y. Masue, R.H. Loeppert, T.A. Kramer, Arsenate and arsenite adsorption and desorption behavior on coprecipitated aluminum: iron hydroxides, *Environ. Sci. Technol.* 41 (3) (2007) 837–842.
- [26] Y. Jin, F. Liu, M. Tong, Y. Hou, Removal of arsenate by cetyltrimethylammonium bromide modified magnetic nanoparticles, *J. Hazard. Mater.* 227 (2012) 461–468.
- [27] J. Mayo, C. Yavuz, S. Yean, L. Cong, H. Shipley, W. Yu, J. Falkner, A. Kan, M. Tomson, V. Colvin, The effect of nanocrystalline magnetite size on arsenic removal, *Sci. Technol. Adv. Mater.* 8 (1–2) (2007) 71.
- [28] R.E. Treybal, *Mass Transfer Operations*, New York, 1980.

- [29] X. Yu, S. Tong, M. Ge, J. Zuo, C. Cao, W. Song, One-step synthesis of magnetic composites of cellulose@iron oxide nanoparticles for arsenic removal, *J. Mater. Chem. A* 1 (3) (2013) 959–965.
- [30] L. Feng, M. Cao, X. Ma, Y. Zhu, C. Hu, Superparamagnetic high-surface-area  $\text{Fe}_3\text{O}_4$  nanoparticles as adsorbents for arsenic removal, *J. Hazard. Mater.* 217 (2012) 439–446.
- [31] F. Mou, J. Guan, H. Ma, L. Xu, W. Shi, Magnetic iron oxide chestnutlike hierarchical nanostructures: preparation and their excellent arsenic removal capabilities, *ACS Appl. Mater. Interfaces* 4 (8) (2012) 3987–3993.
- [32] Y.M. Zheng, S.F. Lim, J.P. Chen, Preparation and characterization of zirconium-based magnetic sorbent for arsenate removal, *J. Colloid Interface Sci.* 338 (1) (2009) 22–29.
- [33] J.P. Chen, *Decontamination of Heavy Metals*, 2012.
- [34] A.M. Showkat, Y.P. Zhang, S.K. Min, A.I. Gopalan, K.R. Reddy, K.P. Lee, Analysis of heavy metal toxic ions by adsorption onto amino-functionalized ordered mesoporous silica, *Bull. Korean Chem. Soc.* 28 (11) (2007) 1985–1992.
- [35] O.F. Sarioglu, N.O.S. Keskin, A. Celebioglu, T. Tekinay, T. Uyar, Bacteria encapsulated electrospun nanofibrous webs for remediation of methylene blue dye in water, *Colloids Surf., B* 152 (2017) 245–251.
- [36] K.R. Reddy, V.G. Gomes, M. Hassan, Carbon functionalized  $\text{TiO}_2$  nanofibers for high efficiency photocatalysis, *Mater. Res. Express* 1 (1) (2014) 015012.
- [37] K.R. Reddy, K. Nakata, T. Ochiai, T. Murakami, D.A. Tryk, A. Fujishima, Facile fabrication and photocatalytic application of Ag nanoparticles- $\text{TiO}_2$  nanofiber composites, *J. Nanosci. Nanotechnol.* 11 (4) (2011) 3692.
- [38] K.R. Reddy, M. Hassan, V.G. Gomes, Hybrid nanostructures based on titanium dioxide for enhanced photocatalysis, *Appl. Catal. A* 489 (2015) 1–16.
- [39] A. Gupta, V.S. Chauhan, N. Sankararamkrishnan, Preparation and evaluation of iron-chitosan composites for removal of As(III) and As(V) from arsenic contaminated real life groundwater, *Water Res.* 43 (15) (2009) 3862–3870.
- [40] T. Li, Z. Zhu, D. Wang, C. Yao, H. Tang, Characterization of floc size, strength and structure under various coagulation mechanisms, *Powder Technol.* 168 (2) (2006) 104–110.
- [41] N. Mahanta, J.P. Chen, A novel route to the engineering of zirconium immobilized nano-scale carbon for arsenate removal from water, *J. Mater. Chem. A* 1 (30) (2013) 8636–8644.
- [42] M.C. Biesinger, B.P. Payne, A.P. Grosvenor, L.W. Lau, A.R. Gerson, R.S.C. Smart, Resolving surface chemical states in XPS analysis of first row transition metals, oxides and hydroxides: Cr, Mn, Fe, Co and Ni, *Appl. Surface Sci.* 257 (7) (2011) 2717–2730.
- [43] D. Wilson, M. Langell, XPS analysis of oleylamine/oleic acid capped  $\text{Fe}_3\text{O}_4$  nanoparticles as a function of temperature, *Appl. Surf. Sci.* 303 (2014) 6–13.
- [44] S.F. Lim, Y.M. Zheng, S.W. Zou, J.P. Chen, Removal of copper by calcium alginate encapsulated magnetic sorbent, *Chem. Eng. J.* 152 (2–3) (2009) 509–513.